J Mater Sci (2010) 45:1154–1159
DOI 10.1007/s10853-009-4036-0

Evidence for a threshold in the biosolubility of aluminosilicate vitreous fibers

François Devreux · Céline Cailleteau · Philippe Barboux

Received: 21 October 2009 / Accepted: 10 November 2009 / Published online: 11 December 2009

Abstract Two series of aluminosilicate glasses have been synthesized with the nominal composition $(64 - x)$ SiO_2–x Al_2O_3–36 Na_2O/CaO with x varying from 9 to 19 mol%. They have been corroded in static conditions in a solution that mimics in a simplified manner the intracellular medium of the lung alveolar macrophages (37 °C, pH 4.6, citric acid). The original and corroded glasses have been studied by ^{27}Al and ^{29}Si MAS NMR. Both series display a sharp increase in the silicon dissolution rate with the alumina content. The glass network dissolves extremely slowly, whereas the release of excess sodium is very fast, for the glasses with low alumina content. On the opposite, the glasses with high alumina content dissolve much more rapidly in a nearly congruent manner. The crossover between the two behaviors occurs for $x = 13$, which corresponds to 33% of aluminum in the glass-former network. The sharp crossover from slow to fast network dissolution is explained in terms of connectivity of the silica sub-network. Above a certain amount of alumina, the silicon sub-network is no more percolating and the corroded glass breaks up into colloids. The sharpness of the transition and the relatively low alumina content required for fast dissolution are related to a structural feature of the aluminosilicate glasses, namely the aluminum self-avoidance that decreases the connectivity of the silica sub-lattice.

F. Devreux (✉) · C. Cailleteau · P. Barboux
Physique de la Matière Condensée, Ecole Polytechnique-CNRS, 91128 Palaiseau, France
e-mail: francois.devreux@polytechnique.fr

Present Address:
C. Cailleteau
SPrAM, INAC, CEA, 17 Avenue des Martyrs, 38054 Grenoble Cedex 9, France

Present Address:
P. Barboux
LCAES, ENSCP-CNRS, 11 rue Pierre et Marie Curie, 75005 Paris, France

Introduction

The asbestos tragedy raised concerns about the possible health effects of the mineral vitreous fibers used as asbestos substitutes for insulation or material reinforcing [1–3]. The innocuity of fibers is mainly assessed by exposing rodents to fiber inhalation or intratracheal instillation and making statistics either on the development of disease [4–6] or on the persistence of fibers in the lung [7–9]. As both involve animal killing, it is highly desirable to dispose of scientific bases to design materials with chemical compositions that warrant fiber biosolubility. Various empiric rules have been proposed based on both in vivo tests and in vitro dissolution experiments [10–13].

Several mechanisms are responsible for the clearance of the fibers inhaled and deposited in the lung [1, 2]. The fibers that are short enough (<20 μm) to be fully engulfed by the alveolar macrophages are phagocytized and transported toward the upper airways through the ciliary escalator. The long fibers can be dissolved in the lung extracellular fluid. They can also be broken into shorter fibers [14] after partial dissolution by the macrophages that attach themselves onto the fibers [15, 16]. Since the pH of the macrophage phagolysosomes is lower than the extracellular one (4.5 vs. 7.4), variant dissolution mechanisms are possible. In particular, the so-called high temperature (HT) stone wool fibers with high alumina content, which are hardly dissolved in the nearly neutral extracellular fluid, become easily soluble in the acidic conditions of the macrophage internal medium [17–21]. In order to

determine the amount of alumina required to make this mechanism efficient, we studied the dissolution of two series of glasses obtained by varying systematically the alumina-silica ratio. The dissolution was performed in a solution which mimics in a simplified manner the internal fluid of the phagolysosomes.

Experimental

The nominal glass compositions were $(64 - x)$ SiO_2–x Al_2O_3–36 Na_2O and $(64 - x)$ SiO_2–x Al_2O_3–36 CaO, where x ranged from 9 to 19 mol%. The glasses were prepared by mixing appropriate amounts of reagent grade silica, alumina, and sodium or calcium carbonate. The fabrication consisted in an intermediate step at 1050 °C for removing carbon dioxide and a final step at 1500 °C for melting the glasses. The glasses were quenched by pouring onto a copper plate or by dipping the platinum crucible in water when the viscosity was too high for pouring. Then, they were ground into small pieces, mechanically milled in an agate mortar and screened to produce different size fractions. The fraction 80–120 μm was used in the experiments. Tables 1 and 2 give the actual glass composition as measured by induced coupled plasma-atomic emission spectroscopy (ICP-AES) and the specific surface area of the calibrated powders as measured by krypton gas adsorption according to the BET method.

Table 1 Compositions and specific surface area of the calibrated powders for the sodium glasses

x	SiO_2		Al_2O_3		Na_2O		Σ (cm^2 g^{-1})
	mol%	wt%	mol%	wt%	mol%	wt%	
9	54.8	51.1	8.7	13.8	36.5	35.2	368
11	52.6	48.4	10.8	16.9	36.6	34.7	497
13	52.0	47.3	12.6	19.4	36.5	33.3	497
15	49.2	44.2	14.7	22.4	36.0	33.4	434
17	46.0	40.9	16.1	24.1	38.0	34.9	429
19	43.6	38.1	19.2	28.4	37.2	33.5	426

Table 2 Composition and specific surface area of the calibrated powders for the calcium glasses

x	SiO_2		Al_2O_3		CaO		Σ (cm^2 g^{-1})
	mol%	wt%	mol%	wt%	mol%	wt%	
9	55.5	53.3	9.3	15.1	35.2	31.6	458
11	53.4	50.9	10.4	17.0	36.2	32.2	468
13	52.0	48.9	12.8	20.4	35.2	30.9	464
15	49.3	45.6	14.8	23.3	35.9	31.1	474
17	48.6	44.4	16.9	26.2	34.5	29.4	455
19	45.9	41.5	18.7	28.6	35.4	29.9	454

Glasses were corroded at 37 °C in static conditions (closed reactor) using 1 g of powder in 450 mL of solution. This makes the S/V (glass surface area-to-solution volume ratio) equal to 1 cm^{-1} owing to the specific surface area of about 450 cm^2 g^{-1}. A constant pH of 4.6 was achieved by using an acetate buffer. Tribasic ammonium citrate (0.5 mmol L^{-1}) was added as a complexing agent since it is known that the formation of aluminum complexes with citric and other organic acids plays a major role in aluminosilicate fiber dissolution [22]. Ammonium salts were preferred to sodium ones with a view to monitor the release of sodium in solution. The solution was periodically sampled (typically 2 mL) to measure the concentrations of the different cations. Silicon, sodium, and aluminum concentrations were measured by colorimetry, flame spectroscopy, and ICP-AES, respectively. The complete kinetics (more than 1 year) was recorded for the sodium glasses, whereas only the initial dissolution regime was monitored for the calcium glasses.

The pristine and corroded glasses were characterized by NMR MAS spectroscopy. The experiments were performed at 93.84 MHz for ^{27}Al and at 73.54 MHz for ^{29}Si. The MAS rotation speed was 10 kHz. The pulse durations were 4 and 10 μs, and the repetition times were 1 and 100 s, for ^{27}Al and ^{29}Si, respectively.

Results

The dissolution rate was calculated from the initial linear variation of silicon concentration versus time:

$$k = \frac{V}{S f_{Si}} \left. \frac{dC_{Si}}{dt} \right|_{t=0}$$

where V is the solution volume, S the initial glass surface area exposed to corrosion, C_{Si} the measured silicon concentration in solution, and f_{si} the silicon mass fraction in the original glass. Figure 1 displays the dissolution rate as a function of alumina content for both series of glasses. The dissolution rates for calcium glasses were systematically lower than the ones for the sodium glasses having the same alumina content. This was expected since the replacement of monovalent Na^+ by divalent Ca^{2+} induces ionic bonds between non-bridging oxygen atoms, which strengthens the network. However, the most impressive were the sharp and parallel increases of the dissolution rates with the alumina content. The glasses with alumina content below 13 mol% displayed a dissolution rate below or around 100 ng cm^{-2} h^{-1}, which is considered as the innocuity threshold [23], whereas glasses with alumina content higher than 14 mol% were fully above.

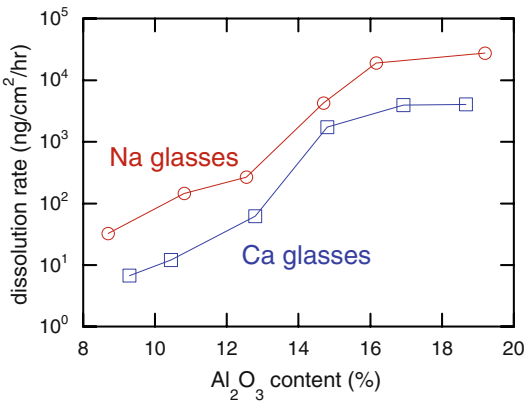

Fig. 1 Variation of the silicon dissolution rate with the alumina content for Na (*circle*) and Ca (*square*) series of glasses

To understand the reason for the rapid change in the dissolution rate, it is useful to consider the complete kinetics. Figure 2 shows the time evolution of Si, Al, and Na leached fractions for the six glasses of the Na series (hereafter designated as *x*Al). The leached fraction is defined for each cation (i = Si, Al, and Na) as the ratio of the dissolved mass (m_i^{d}) to the mass in the original glass (m_i^{g}):

$$\mathrm{LF}_i = \frac{m_i^{\mathrm{d}}}{m_i^{\mathrm{g}}} = \frac{C_i\, V}{f_i\, m}$$

where m is the mass of the glass powder before corrosion. A few significant points stand out from the data in Fig. 2. Firstly, network formers (Si and Al) dissolved almost congruently, except for glass 13Al. Secondly, the release of sodium was very fast compared to network dissolution in the three low alumina glasses (first row). Conversely, the initial dissolution was congruent and sodium continued to be slowly released after silica saturation for the three high alumina glasses (second row). Thirdly, the saturation of the solution with respect to silica was not achieved even after 1 year for the most slowly dissolving glass (9Al). It was reached more or less rapidly, but monotonously, for samples 11Al to 15Al, for which the final silicon concentration (about 40 mg L^{-1}) corresponds quite well to the silica solubility in the present conditions of temperature and pH. On the contrary, there was an important silicon oversaturation for samples 17Al and 19Al, where the concentrations rise up to 90 and 110 mg L^{-1}, respectively, before slowly decreasing to more regular values.

The differences in corrosion mechanisms were also obvious in the structure of the corroded glasses. Figure 3 displays MAS NMR spectra for samples 11Al and 17Al before and after alteration. The position of the ^{27}Al NMR line (chemical shift at 50 ppm) shows that aluminum was in tetrahedral coordination in the original glasses. It remained in the same environment in the altered sample 11Al, whereas part of the aluminum cations became octahedrally coordinated in the altered sample 17Al (chemical shift at 0 ppm). Octahedral aluminum was recently observed in the corrosion of other aluminosilicate glasses and was attributed to an in situ transformation of the

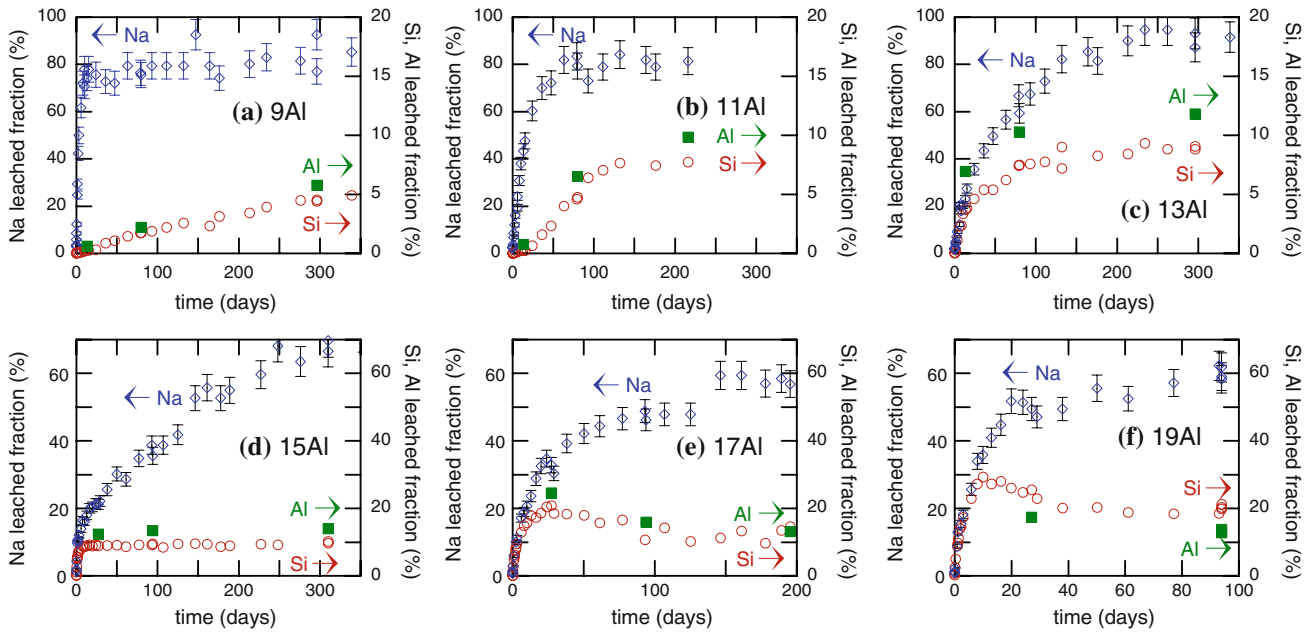

Fig. 2 Corrosion kinetics of the six sodium glasses. The leached fractions of Si (*open circle*), Al (*closed square*), and Na (*open diamond*) are plotted versus time. Note that the *Y*-scale is different for Na (*left*) and Si and Al (*right*) for the glasses of the first row (9Al to 13Al), but is the same for the ones of the second raw (15Al to 19Al). Note also that the time scale is different for samples 17Al and 19Al

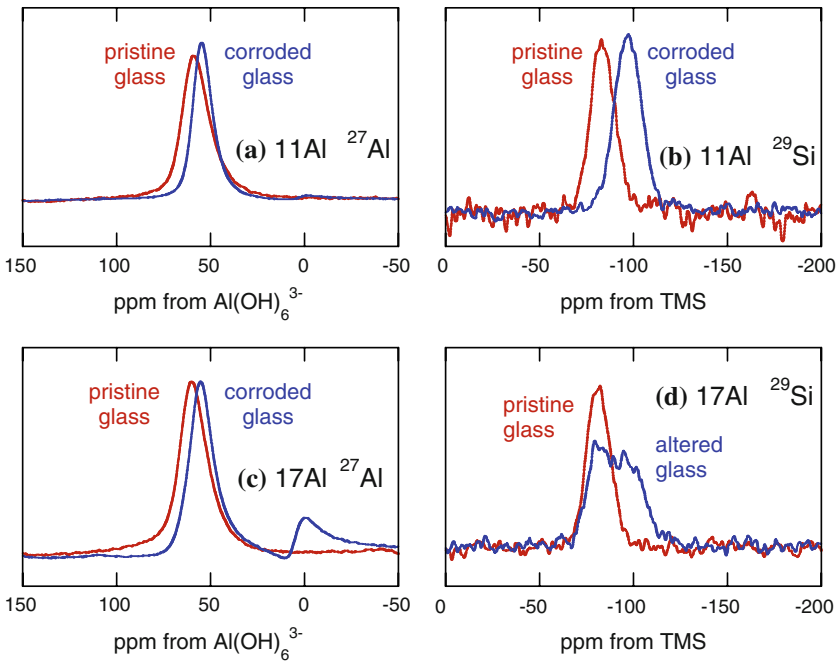

Fig. 3 ^{27}Al and ^{29}Si NMR spectra of glasses 11Al and 17Al before and after corrosion. The spectra of samples 9Al and 13Al looked like the ones of 11Al, whereas those of 15Al and 19Al were alike the ones of 17Al

aluminum environment in the altered layer [24]. In both samples, there was a small upfield shift of the 50 ppm line in corroded glasses, which can be attributed to the restructuring of the glass network. The line shift was much more important in ^{29}Si NMR. The whole line was shifted from −82 to −96 ppm in sample 11Al. The same shift was observed in 17Al but it concerns only 50% of the silicon atoms. These upfield shifts brought out the network repolymerization following the departure of the sodium cations.

Discussion

There is a clear partition of the glasses into two families, regarding both the dissolution kinetics and the structure of the corroded glasses. Samples 9Al to 13Al present a homogeneous structural transformation as highlighted by NMR and by the fast release of 80–90% of sodium. The remaining sodium atoms are expected to play the role of charge-balancing cations for AlO_4^- units. This transformation is followed by the slow dissolution of the vitreous network. On the contrary, a core of unaltered glass coexists with a corroded surface crown after the fast initial dissolution in samples 15Al to 19Al. Interestingly, the release of sodium through the corroded layer is much slower than through the unaltered network of the low alumina glasses. This is a consequence of the restructuring and the densification of the corroded layer, which inhibit or at least slow down the transport of soluble cations [25, 26]. The dissolution rate variation is clearly not controlled by the degree of polymerization of the vitreous network, since the number of non-bridging oxygens *decreases* as alumina content increases (Table 3). We rather propose that the difference between low alumina glasses (slow and highly non-congruent dissolution) and high alumina glasses (fast and congruent dissolution) is related to the connectivity of the silica sub-lattice. When this sub-lattice becomes non-percolating owing to the increase in alumina content, small clusters can be easily disconnected from the glass surface after dissolution of the surrounding aluminum atoms. This should lead to a disintegration of the glass surface in the form of small colloids. This view is supported by the silica oversaturation observed in samples 17Na and 19Na (Fig. 2e, f). It is relevant to notice that silica oversaturation has been already observed in some minerals (pseudowollastonite, β-$CaSiO_2$) as a direct consequence of the presence of small-sized isolated clusters in the structure of the material [27].

Table 3 Structural characteristics of the vitreous networks

x	Na glasses		Ca glasses	
	R_{NBO}	R_{Al}	R_{NBO}	R_{Al}
9	0.77	0.24	0.70	0.25
11	0.69	0.29	0.69	0.28
13	0.59	0.33	0.58	0.33
15	0.54	0.37	0.54	0.38
17	0.57	0.41	0.43	0.41
19	0.44	0.47	0.40	0.45

R_{NBO} is the number of non-bridging oxygen per tetrahedron and R_{Al} is the proportion of aluminum among the glass network formers

Percolation has been already invoked in the corrosion of sodium borosilicate glasses [28–30], where boron plays the same role as aluminum in the present case. The relevant parameter is the proportion of soluble cations among the glass network formers:

$$R_M = \frac{[M]}{[Si] + [M]} = \frac{2[M_2O_3]}{[SiO_2] + 2[M_2O_3]}$$

where M can be either Al or B (the actual R_{Al} values are given in Table 3). There are two percolation transitions: one for the M sub-lattice at $R_M = p_c$, and another one for the silica sub-lattice at $R_M = 1 - p_c$. Assuming p_c smaller than 0.5, the transitions define three domains that present distinct behaviors with respect to corrosion. At low M_2O_3 content $(R_M < p_c)$, the clusters of directly connected M tetrahedrons are finite in size. Thus, the dissolution of the M sub-lattice requires the one of silica, which makes the *network* dissolution congruent. In the intermediate domain $(p_c < R_M < 1 - p_c)$, both sub-lattices are percolating. The soluble network-former cations can be selectively extracted without silica dissolution. Finally, at high M_2O_3 content $(R_M > 1 - p_c)$, the silica sub-lattice is no more percolating and thus small glass fragments can be dissolved as colloidal particles. The *whole glass* dissolution is congruent. In borosilicates, the first transition arises for $R_B^1 \approx 0.40$ [29] and the second one was found around $R_B^2 \approx 0.57$ [28]. Both results agree with a p_c value close to the percolation threshold for the diamond lattice ($p_c = 0.39$ and 0.42 for bond and site percolations, respectively), which presents the same coordination number as the tetrahedral glass network.

In the present case, the transition to colloidal dissolution takes place at much lower aluminum content. The borderline between slow and fast dissolution occurs around 13 mol% Al_2O_3, which corresponds to $R_{Al}^2 \approx 0.33$ (Table 1) instead of 0.57 for borosilicates. This low value can be explained by a specific structural feature of the aluminosilicate glasses. Actually, in standard percolation theory, the two species are supposed to be *randomly* distributed on the lattice sites. It is well known that this is not true for the Si and Al tetrahedrons in aluminosilicate glasses [21, 22]. According to Loewenstein's rule [31], there is an aluminum self-avoidance in these glasses. This increases the relative amount of Si tetrahedrons required for the percolation of the silica sub-lattice. Indeed, the proportion of Si–O–Si bonds is no more $1 - R_{Al}$, but $1 - 2R_{Al}$ in case of perfect self-avoidance. Then, the bond percolation of the silicon sub-lattice should disappear for $1 - 2R_{Al} < p_c$, that is for $R_{Al} > 0.31$ instead of 0.61 for random percolation. The small difference with the experimental value (0.33) can be explained by an incomplete Al-avoidance. Furthermore, the intermediate regime where both sub-lattices are percolating does not exist at all for perfect Al-avoidance, and should be quite limited in case of incomplete avoidance. It would correspond to sample 13Al, which is the only glass having non-congruent Si and Al dissolution (Fig. 2c). The almost absence of the intermediate regime also explains the sharp partition in soluble and insoluble glasses for aluminosilicates, whereas a smooth transition was observed in borosilicates [29].

Conclusion

It has been demonstrated that it exists a sharp threshold in alumina content to insure the fast dissolution of the aluminosilicate glasses in weakly acidic conditions. Moreover, it has been shown that the low value of the threshold is a direct consequence of the specific structure of aluminosilicate glasses. The similar variations of the dissolution rates for the Na and Ca series of glasses indicate that the transition is an intrinsic property of the aluminosilicate network. The dissolution rates measured for the calcium series are in general agreement with the measurements made on commercial HT stone wool fibers that contain a significant amount of earth-alkali oxides (mainly Ca and Mg) and a much smaller amount of alkali oxides [19–21]. However, the sharp transition between slowly and rapidly dissolving glasses is much more visible in this study because of the controlled glass composition, whereas commercial fibers contain variable amounts of different oxides, which partly blurs the variation of the dissolution rate with respect to alumina content.

References

1. Hesterberg TW, Hart GA (2001) Crit Rev Toxicol 31:1
2. Maxim LD, Hadley JG, Potter RM, Niebo R (2006) Regul Toxicol Pharmacol 46:42
3. Bernstein DM (2007) Crit Rev Toxicol 37:839
4. Miller BG, Searl A, Davis JMG, Donaldson K, Cullen RT, Bolton RE, Buchanan D, Soutar CA (1999) Ann Occup Hyg 43:155
5. Miller BG, Jones AD, Searl A, Buchanan D, Cullen RT, Soutar CA, Davis JMG, Donaldson K (1999) Ann Occup Hyg 43:167
6. Bellmann B, Muhle H, Creutzenberg O, Ernst H, Muller M, Bernstein DM, Sintes JMR (2003) Inhal Toxicol 15:1147
7. Bernstein DM, Morscheidt C, Grimm HG, Thevenaz P, Teichert U (1996) Inhal Toxicol 8:345
8. Hesterberg TW, Chase G, Axten C, Miller WC, Musselman RP, Kamstrup O, Hadley J, Morscheidt C, Bernstein DM, Thevenaz P (1998) Toxicol Appl Pharmacol 151:262
9. Searl A, Buchanan D, Cullen RT, Jones AD, Miller BG, Soutar CA (1999) Ann Occup Hyg 43:143
10. Eastes W, Potter RM, Hadley JG (2000) Inhal Toxicol 12:269
11. Eastes W, Potter RM, Hadley JG (2000) Inhal Toxicol 12:1127
12. de Meringo A, Lafon F, Furtak H, Hanton D (2000) Glass Sci Technol Glasstesch Ber 73:79
13. Ohsawa M, Misu Y (2003) Glass Sci Technol 76:263

14. Eastes W, Baron PA, Baier RE, Guldberg M, Potter R (2007) Inhal Toxicol 19:311
15. Luoto K, Holopainen M, Kangas J, Kallilkosko P, Savolainen K (1995) Environ Res 70:51
16. Nguea HD, Rhin B, Mahon D, Bernard JL, De Reydelet A, Le Faou A (2005) Arch Toxicol 79:487
17. Bellmann B, Muhle H, Kamstrup O, Draeger UF (1995) Exp Toxicol Pathol 47:195
18. Knudsen T, Guldberg M, Christensen VR, Jensen SL (1996) Glass Sci Technol Glasstesch Ber 69:331
19. Guldberg M, Christensen VR, Perander M, Zoitos B, Koenig AR, Sebastian K (1998) Ann Occup Hyg 42:233
20. Guldberg M, de Meringo A, Kamstrup O, Furtak H, Rossiter C (2000) Regul Toxicol Pharmacol 32:184
21. Guldberg M, Jensen SL, Knudsen T, Steenberg T, Kamstrup O (2002) Regul Toxicol Pharmacol 35:217
22. Steenberg T, Hjenner HK, Jensen SL, Guldberg M, Knudsen T (2001) Glass Sci Technol Glasstesch Ber 74:97
23. Eastes W, Hadley JH (1996) Inhal Toxicol 8:323
24. Tsomaia N, Brantley SL, Hamilton JP, Pantano CG, Mueller KT (2003) Am Mineral 88:54
25. Devreux F, Barpoux P, Filoche M, Sapoval B (2001) J Mater Sci 36:1331. doi:10.1023/A:1017591100985
26. Cailleteau C, Angeli F, Devreux F, Gin S, Jestin J, Jollivet P, Spalla O (2008) Nat Mater 7:978
27. Casey WH (2008) Nat Mater 7:930
28. Kinoshita M, Harada M, Sato Y, Hariguchi Y (1991) J Am Ceram Soc 74:783
29. Ledieu A, Devreux F, Barboux P, Sicard L, Spalla O (2004) J Non-Cryst Solids 343:3
30. Devreux F, Ledieu A, Barboux P, Minet Y (2004) J Non-Cryst Solids 343:13
31. Loewenstein W (1954) Am Mineral 39:92